Geomechanics and Engineering, *Vol. 34, No. 1 (2023) 69-86*
https://doi.org/10.12989/gae.2023.34.1.069

A secondary development based on the Hoek-Brown criterion for rapid numerical simulation prediction of mountainous tunnels in China

Jian Zhou*[1,2,3], Xinan Yang[4a] and Zhi Ding[1,2,3b]

[1]*Department of Civil Engineering, Hangzhou City University, Hangzhou 310015, China*
[2]*Zhejiang Engineering Research Center of Intelligent Urban Infrastructure, Hangzhou City University, Hangzhou 310015, China*
[3]*Key Laboratory of Safe Construction and Intelligent Maintenance for Urban Shield Tunnels of Zhejiang Province, Hangzhou City University, Hangzhou 310015, China*
[4]*The Key Laboratory of Road and Traffic Engineering, Ministry of Education, Tongji University, Shanghai 201804, China*

(*Received November 14, 2022, Revised April 25, 2023, Accepted May 16, 2023*)

Abstract. To overcome the dilemma of the [BQ] method's inability to predict mountain tunnel support loads, this study is based on the Hoek-Brown criterion and previous results to obtain the connection equations from GSI scores to each parameter of the Hoek-Brown criterion and the link between the [BQ] scores and the GSI system. The equations were embedded in the Hoek-Brown criterion of FLAC6.0 software to obtain tunnel construction forecasts without destroying the in-situ stratigraphy. The feasibility of the secondary development of the Hoek-Brown criterion was verified through comparative analysis with field engineering measurements. If GSI > 45 with a confining pressure of less than 10 MPa, GSI has little effect on the critical softening factor while we should pay attention to the parameter of confining pressure when GSI < 45. The design values for each parameter are closer to the FLAC3D simulation results and the secondary development of the Hoek-Brown criterion meets the design objectives. If the Class V surrounding rock is thinned with shotcrete or the secondary lining is installed earlier, the secondary lining may act as the main load-bearing structure. The study may provide ideas for rapid prediction of mountainous tunnels in China.

Keywords: [BQ]; confining pressure; GSI; Hoek-Brown criterion; mountain tunnel

1. Introduction

Hoek created the GSI rock classification system that who with Brown proposed the non-linear Hoek-Brown (H-B) criterion based on extensive tests, which is widely used in rock engineering (Merifield *et al*. 2006, Cai 2010, Yang *et al*. 2018, Ismael and Konietzky 2019, Zareifard 2020, Ranjbarnia *et al*. 2021, Gomes *et al*. 2021). For mountain tunnels, the non-linear characteristics and the significant post-peak strain-softening of the rock have been recognized by many scholars as the dominant constitutive model for mountain tunneling (Bagheripour *et al*. 2011, Zou *et al*. 2016, Ukritchon and Keawsawasvong 2019, Li and Yang 2019, Chinaei *et al*. 2021, Wu *et al.* 2021a, b, Zhao *et al.* 2023a, b).

Currently, Hoek-Brown criterion, as an empirical criterion, has some obstacles in how to predict the construction of mountain tunnels. The use of Hoek Brown criterion mainly includes theoretical analysis and numerical simulation (Wu *et al.* 2022a, b). As the theoretical formula is too complex and extremely strict on the parameters, the calculation results are difficult to be more consistent with the field monitoring, which is not conducive to the promotion in engineering practice (Wu and Shao 2019, Wu *et al.* 2020, Zhao *et al.* 2022a, b). Numerical simulation tool is low cost, which can predict such as surrounding rock deformation and stresses in tunneling projects with a high degree of accuracy. The application of the generalized Hoek- Brown criterion to numerical simulations has been researched by some scholars. Cai *et al*. (2022) established a three-dimensional (3D) numerical model for deep tunneling for a typical tunnel in western China to study the 3D-nonlinear spatial effects and mechanisms during excavation with incorporation of the 3D Hoek-Brown strength criterion. Xu *et al*. (2022) put forward a novel fractional damage visco-plastic model to describe the creep response of rocks with the following elements: (1) an Abel dashpot, (2) a damaged Abel dashpot coupled with damage formulation that is based on a statistical distribution of microfractures, (3) elastic spring, and (4) Hoek-Brown plastic element. Huang *et al*. (2021) investigated the stability of deep rectangular tunnels excavated in a jointed rock mass using adaptive finite element limit analysis (AFELA) method. Kabwe *et al*. (2019) presented an analytical solution which considers non-circular tunnels and the intermediate principal stress. A numerical simulation is conducted in FLAC(3D) to verify the presented solution with a native constitutive model for a chosen rock mass condition. The above results lack the simulation of the properties of the surrounding rock, especially the simulation of the transition from an elastic to a plastic or even fractured state due to tunnel excavation. This necessarily

*Corresponding author, Ph.D.
E-mail: zhoujian@hzcu.edu.cn
[a]Professor
[b]Professor

ISSN: 2005-307X (Print), 2092-6219 (Online)

involves the secondary development of the constitutive model.

Numerical simulations should incorporate geological features within the geotechnical materials (Han *et al*. 2022, Gu *et al*. 2022, Gu *et al*. 2023). The discontinuities within the surrounding rock (e.g. jointed fractures, softening, non-linearity, etc.) are generally characterized by modifying the constitutive relationships (Qin *et al.* 2023, Wu *et al.* 2023a, b). Li (2012) verified the feasibility of the model by developing a two-dimensional constitutive model of the rock which used column compression tests and applied the model to excavation simulations of shallow buried tunnels. The results show that the new constitutive model can reflect the whole process of rock structure from local plastic deformation to overall rupture, and the calculated results are in good agreement with the experiments. Zhu (2015) established a rock damage constitutive model for fine view damage by secondary development of a custom constitutive model in C++ language, and verified the reasonableness of the theoretical model by uniaxial compression numerical tests on rock specimens. Based on the FLAC3D finite difference software, Wang (2018) established an elastoplastic coupled strain-softening model by considering the surrounding pressure and plastic shear strain which compared the simulation results with the experimental data to verify the feasibility of the secondary developed model. Jin *et al*. (2020) embedded the brittle drop constitutive integral algorithm of Hoek-Brown criterion reflecting strain softening into the finite element software ABAQUS. The strain-softening analytical solution was compared with the finite element solution and found to be in good agreement. Although this part of the results provides a secondary development of the present model, the development requires precise parameters for the rock, which need to be determined through extensive experimentation. From another point of view, the above development methods require very accurate rock and geological parameters, which take a lot of time and cost to obtain. These methods are not normally used in engineering practice. Therefore, if a secondary development method for rapid prediction of tunnel stability could be found, it could provide a quantitative prediction for the construction of mountainous tunnels based on the [BQ] method of surrounding rock classification.

Similar to the GSI (Geological Strength Index) system, the rock classification system based on [BQ] method (a classification method of surrounding rock in China) has been formed in the Chinese region with a large number of summaries of factors such as the hardness and integrity of the surrounding rock which has been incorporated into the specifications to guide the project. In-situ sampling to obtain rock parameters by laboratory testing actually destroys the in-situ stratigraphy and the parameters obtained are actually inaccurate. Many scholars have sought to achieve a high degree of accuracy by secondary development around the damage and softening properties of rocks, which must be based on very precise parameters. In contrast, numerical simulation is a predictive tool, and the numerical simulation results are considered successful when the error between the numerical simulation results and the field monitoring is kept as small as possible. The paper plans a secondary development from another perspective which seeks to obtain an equivalent method for the GSI scores to the [BQ] scores and embeds in the Hoek-Brown criterion to obtain numerical simulation results that preserve the in-situ nature of the formation. Currently, several European rock classification systems are linked in part by scholars who have carried out equivalence formulas. Laderian and Abaspoor (2012) deemed that the best correlation coefficient between RMR and Q system was determined with the aim of suggesting a new potential correlation for various geotechnical activities in parts of Iran. Somodi *et al*. (2021) presented linear equations for estimating GSI from measured RMR values. Bertuzzi *et al*. (2016) proposed to quantify GSI with RQD and the joint condition rating of RMR. It is recommended that the quantified GSI approach be used to supplement and check the visually assessed chart GSI. Campos *et al*. (2020) developed the RMR with the aim of recommending conceptual engineering solutions, while the purpose of the GSI is to estimate the strength and deformability parameters of rock masses. Those set the stage for finding a link between the GSI system and the [BQ] system.

Based on the above, this study plans to equate the GSI with the [BQ] analysis and find the connection between the parameters of the GSI and the Hoek-Brown criterion in order to modify the Hoek-Brown criterion constitutive model of the FLAC3D6.0 software in the form of a function. Numerical simulations are then analyzed and validated with measured data.

2. Hoek-Brown strength criterion

The Mohr-Coulomb criterion is based on the plastic state of the intact rock mass, which ignores factors such as joints, fractures and excavation disturbances in the rock mass itself. The Hoek-Brown strength criterion compensates for these shortcomings better. The Hoek-Brown strength criterion has been continually revised to form the generalized Hoek-Brown yielding criterion as (Hoek *et al*. 2002)

$$\sigma_1=\sigma_3+\sigma_{\mathrm{ci}}\left(m_{\mathrm{b}}\frac{\sigma_3}{\sigma_{\mathrm{ci}}}+s\right)^a \tag{1}$$

where σ_1 and σ_3 represent the maximum and minimum principal stresses on the yield surface respectively. σ_{ci} is the uniaxial compressive strength of the rock mass. m_{b}, s and a are material parameters of the rock mass, which can be characterized by the GSI as

$$\begin{cases} m_{\mathrm{b}}^{\mathrm{p}}=m_{\mathrm{i}}\exp\left(\dfrac{\mathrm{GSI}^{\mathrm{p}}-100}{28-14D}\right) \\ s^{\mathrm{p}}=\exp\left(\dfrac{\mathrm{GSI}^{\mathrm{p}}-100}{9-3D}\right) \\ a^{\mathrm{p}}=\dfrac{1}{2}+\dfrac{1}{6}\left[\exp\left(\dfrac{-\mathrm{GSI}^{\mathrm{p}}}{15}\right)-\exp\left(\dfrac{-20}{3}\right)\right] \end{cases} \tag{2}$$

$$\begin{cases} m_{\mathrm{b}}^{\mathrm{r}} = m_{\mathrm{i}} \exp\left(\dfrac{\mathrm{GSI}^{\mathrm{r}} - 100}{28 - 14D}\right) \\ s^{\mathrm{r}} = \exp\left(\dfrac{\mathrm{GSI}^{\mathrm{r}} - 100}{9 - 3D}\right) \\ a^{\mathrm{r}} = \dfrac{1}{2} + \dfrac{1}{6}\left[\exp\left(\dfrac{-\mathrm{GSI}^{\mathrm{r}}}{15}\right) - \exp\left(\dfrac{-20}{3}\right)\right] \end{cases} \tag{3}$$

where 'p' and 'r' are the distinguishing marks for the softening and residual zones. m_{i} is the material constant for intact rock. D indicates the disturbance degree of rock mass, which is taken between 0 and 1. The greater the value of D, the greater the disturbance.

Cai *et al*. (2007) obtained the relationship between $\mathrm{GSI}^{\mathrm{r}}$ in the residual zone of the surrounding rock and GSI based on in-situ rock shear tests as

$$\mathrm{GSI}^{\mathrm{r}} = \mathrm{GSI}\exp(-0.0134\mathrm{GSI}) \tag{4}$$

The H-B criterion can be transformed into an equation containing the softening parameter η when the surrounding rock exhibits strain softening (Hoek *et al*. 2002).

$$f(\sigma_r, \sigma_\theta, \eta) = \sigma_\theta - \sigma_r - \sqrt{m(\eta)\sigma_r\sigma_{\mathrm{ci}} + s(\eta)\sigma_{\mathrm{ci}}^2} \tag{5}$$

where η is the plastic softening coefficient of the surrounding rock, which can be expressed by the plastic shear strain. It is assumed that the tunnel is in a hydrostatic stress field with a uniform load, η can be expressed as the difference between the plastic tangential strain and the radial strain, with the expression (Wang *et al*. 2010) as

$$\eta = \varepsilon_\theta^{\mathrm{p}} - \varepsilon_r^{\mathrm{p}} \tag{6}$$

where $\varepsilon_\theta^{\mathrm{p}}$ and $\varepsilon_r^{\mathrm{p}}$ are plastic tangential and radial strains respectively.

The strength parameter ω (m_b, s and α) is a segmented linear function of η and its relationship to the different elastoplastic models can be determined as shown in Fig. 1. η^* is the critical softening parameter. The specific expressions are as follows.

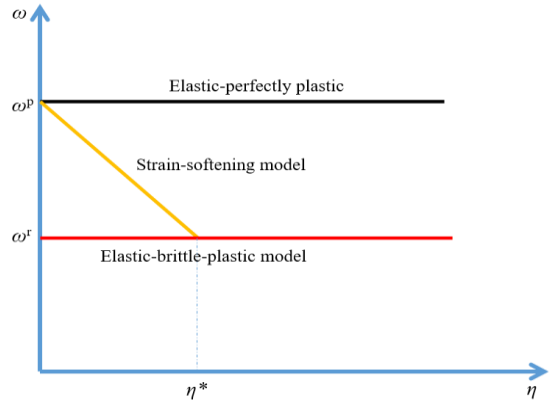

Fig. 1 Relationship between strength parameters and softening factor for different models

Elastic-brittle-plastic model

$$\omega(\eta) = \omega^{\mathrm{r}} \tag{7}$$

Strain-softening model:

$$\omega_1(\eta) = \begin{cases} \omega_1^{\mathrm{p}} - \left(\omega_1^{\mathrm{p}} - \omega_1^{\mathrm{r}}\right)\dfrac{\eta}{\eta^*} & 0 < \eta < \eta^* \\ \omega_1^{\mathrm{r}} & \eta \geq \eta^* \end{cases} \tag{8}$$

Elastic-perfectly plastic model:

$$\omega(\eta) = \omega^{\mathrm{p}} \tag{9}$$

where ω_1 is the strength parameter related to m_b, s and α. ω_1^{p} and ω_1^{r} correspond to the strength parameters of surrounding rock in softening zone and residual zone respectively. Alejano et al. (2010) proposed a formula for η^* based on the full stress-strain curve and the results of tri-axial tests on a large number of weathered rocks.

$$\eta^* = M\frac{\sigma_{\mathrm{ci}}}{E}\left[\left(m_{\mathrm{b}}^{\mathrm{p}}\frac{\sigma_3}{\sigma_{\mathrm{ci}}} + s^{\mathrm{p}}\right)^{a^{\mathrm{p}}} - \left(m_{\mathrm{b}}^{\mathrm{r}}\frac{\sigma_3}{\sigma_{\mathrm{ci}}} + s^{\mathrm{r}}\right)^{a^{\mathrm{r}}}\right]\left(1 + \frac{K_\psi}{2}\right) \tag{10}$$

where

$$M = \begin{cases} 1 + \dfrac{\sigma_3 / \left(2\sqrt{s^{\mathrm{p}}}\sigma_{\mathrm{ci}}\right) + 0.05}{0.0046e^{0.0768\mathrm{GSI}^{\mathrm{p}}}} & \dfrac{\sigma_3}{\sqrt{s^{\mathrm{p}}}\sigma_{\mathrm{ci}}} \leq 0.1 \\ 1 + \dfrac{\sigma_3 / \left(\sqrt{s^{\mathrm{p}}}\sigma_{\mathrm{ci}}\right)}{0.0046e^{0.0768\mathrm{GSI}^{\mathrm{p}}}} & \dfrac{\sigma_3}{\sqrt{s^{\mathrm{p}}}\sigma_{\mathrm{ci}}} > 0.1 \end{cases}$$

. σ_3 is the third principal stress, i.e. confining pressure. $K_\psi$can be expressed as

$$\begin{cases} K_\psi = 1 + \left(K_\psi^{\mathrm{p}} - 1\right)e^{-\frac{\eta}{\eta^*}} \\ K_\psi^{\mathrm{p}} = \left(1 + \sin\psi^{\mathrm{p}}\right)/\left(1 - \sin\psi^{\mathrm{p}}\right) \\ \psi^{\mathrm{p}} = \dfrac{\arcsin\dfrac{Q}{Q+2}}{1 + \lg\sigma_{\mathrm{ci}}}\lg\dfrac{\sigma_{\mathrm{ci}}}{\sigma_3 + 0.1} \\ Q = a^{\mathrm{p}}m_{\mathrm{b}}^{\mathrm{p}}\left(m_{\mathrm{b}}^{\mathrm{p}}\dfrac{\sigma_3}{\sigma_{\mathrm{ci}}} + s^{\mathrm{p}}\right)^{a^{\mathrm{p}}-1} \end{cases} \tag{11}$$

where m_{i} denotes the material constant of intact rock. Cui *et al*. (2019) obtained the relationship between m_{i} and GSI.

$$m_{\mathrm{i}} = 0.7375\mathrm{GSI}^{0.7586} \tag{12}$$

where GSI is the geological strength index. For the axisymmetric plane strain analysis of a tunnel, the maximum principal stress σ_1 and minimum principal stress σ_3 are equal to the tangential stress and radial stress of surrounding rock, respectively. Thus, Eq. (1) can be rewritten as

$$\sigma_\theta = \sigma_r + \sigma_{\mathrm{ci}}\left(m_{\mathrm{b}}\frac{\sigma_3}{\sigma_{\mathrm{ci}}} + s\right)^a \tag{13}$$

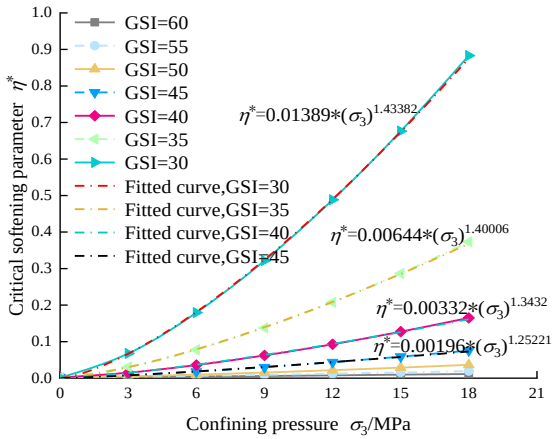

Fig. 2 Curves of the relationship between GSI and η^*

3. Secondary development of constitutive model

3.1 Development process

In order to determine the change paths of post-peak parameters in FLAC3D's own Hoek-Brown-PAC constitutive model, the constitutive model was developed twice. A plastic shear strain with a softening factor of η was defined and a relationship function between the constitutive parameters and the plastic shear strain was constructed. The value of η plays a key role in the yield state of the material when it is in a plastic softening state. The material is in an elastic state when η=0. Focus on situation $0<\eta<\eta^*$, where the material appears to be plastic softening. When $\eta>\eta^*$, the plastic softening property of the material disappears and the material is broken. Cui *et al*. (2019) drew the relationship between GSI and η^* in combination with Hoek and Brown (1997) and Arzua *et al*. (2013, 2014) who believed that when the confining pressure is less than 10 MPa, the confining pressure has little effect on GSI. However, a large number of tri-axial tests of rocks show that for the same kind of rocks with different confining pressures, the softening process of standard specimens with large confining pressure is longer with a larger η^*. Therefore, the influence of confining pressure should be taken account into in the construction of constitutive function to judge whether the confining pressure has obvious effect on the GSI's interval from 25 to 75, or for one of them.

Combining Eqs. (10) and (11), the relationship between GSI and η^* under the different confining pressure can be shown in Fig. 2. It can be seen from Fig. 2 that the critical rock softening parameter η^* tends to increase for a given GSI and the larger the GSI, the more pronounced this trend becomes. The smaller the GSI at a given confining pressure, the greater the η^*, which reflects the obvious softening characteristics of the weak surrounding rock. The effect of GSI on η^* is not significant when the circumferential pressure is equal to 0, and this effect becomes increasingly significant as the circumferential pressure increases. It is worth noting that for GSI > 45, the effect of confining pressure is less important and it is recommended that the effect of confining pressure on η^* can be ignored for confining pressure less than 10 MPa, while the effect of confining pressure should be taken into account for GSI < 45.

From this, the complex form of Eq. (10) can be simplified. With a known GSI, the value of η^* can be expressed in a similar format to the fitted curves in Fig.2, as follows.

$$\eta^* = z_1 \times (\sigma_3)^{z_2} \tag{14}$$

Where z_1 and z_2 are undetermined coefficients, which can be obtained by GSI and σ_3, respectively.

The relationship between softening stage, residual stage and η^* is regarded as a linear relationship. Combined with Eqs. (2)-(11) and (14), the piecewise function between σ_{ci} and η of softening and residual stages can be written as

$$\begin{cases} \sigma_{ci}(\eta) = \dfrac{\dfrac{0.5\exp(0.06\mathrm{GSI}^r)}{0.0387+0.00474\exp(\mathrm{GSI}^r/18.9086)} - \dfrac{0.5\exp(0.06\mathrm{GSI})}{0.0387+0.00474\exp(\mathrm{GSI}/18.9086)}}{z_1\times(\sigma_3)^{z_2}}\eta \\ \quad + \dfrac{0.5\exp(0.06\mathrm{GSI})}{0.0387+0.00474\exp(\mathrm{GSI}/18.9086)} & 0<\eta<z_1\times(\sigma_3)^{z_2} \\ \sigma_{ci}(\eta) = \dfrac{0.5\exp(0.06\mathrm{GSI}^r)}{0.0387+0.00474\exp(\mathrm{GSI}^r/18.9086)} & \eta > z_1\times(\sigma_3)^{z_2} \end{cases} \tag{15}$$

Similarly, let $D = 0$. The functional relationship between parameters m_b, s, a and η can be written respectively as

$$\begin{cases} m_b(\eta) = \dfrac{0.7375(\mathrm{GSI}^r)^{0.7586}\exp\left(\dfrac{\mathrm{GSI}^r-100}{28}\right) - 0.7375(\mathrm{GSI})^{0.7586}\exp\left(\dfrac{\mathrm{GSI}-100}{28}\right)}{z_1\times(\sigma_3)^{z_2}}\eta \\ \quad + 0.7375(\mathrm{GSI})^{0.7586}\exp\left(\dfrac{\mathrm{GSI}-100}{28}\right) & 0<\eta<z_1\times(\sigma_3)^{z_2} \\ m_b(\eta) = 0.7375(\mathrm{GSI}^r)^{0.7586}\exp\left(\dfrac{\mathrm{GSI}^r-100}{28}\right) & \eta > z_1\times(\sigma_3)^{z_2} \end{cases} \tag{16}$$

$$\begin{cases} s(\eta) = \dfrac{\exp\left(\dfrac{\mathrm{GSI}^r-100}{9}\right) - \exp\left(\dfrac{\mathrm{GSI}-100}{9}\right)}{z_1\times(\sigma_3)^{z_2}}\eta + \exp\left(\dfrac{\mathrm{GSI}-100}{9}\right) \\ \qquad\qquad 0<\eta<z_1\times(\sigma_3)^{z_2} \\ s(\eta) = \exp\left(\dfrac{\mathrm{GSI}^r-100}{9}\right) \qquad \eta > z_1\times(\sigma_3)^{z_2} \end{cases} \tag{17}$$

$$\begin{cases} a(\eta) = \dfrac{\dfrac{1}{6}\left\{\left[\exp\left(\dfrac{-\mathrm{GSI}^r}{15}\right)-\exp\left(\dfrac{-20}{3}\right)\right]-\left[\exp\left(\dfrac{-\mathrm{GSI}}{15}\right)-\exp\left(\dfrac{-20}{3}\right)\right]\right\}}{z_1\times(\sigma_3)^{z_2}}\eta \\ \quad +0.5+\dfrac{1}{6}\left[\exp\left(\dfrac{-\mathrm{GSI}}{15}\right)-\exp\left(\dfrac{-20}{3}\right)\right] \quad 0<\eta<z_1\times(\sigma_3)^{z_2} \\ a(\eta) = 0.5+\dfrac{1}{6}\exp\left[\left(\dfrac{-\mathrm{GSI}^r}{15}\right)-\exp\left(\dfrac{-20}{3}\right)\right] \quad \eta > z_1\times(\sigma_3)^{z_2} \end{cases} \tag{18}$$

The Visual Studio 2010 compilation platform was chosen for the secondary development of the Hoek-Brown-PAC constitutive model. A new project in the platform was created and "FLAC3D600 Constitutive Model" was selected. The system generates a user-defined development project with the same name as this structure, called Hoek

Brown PAC. The internal compilation of this constructive model is in C++ language and uses classes to characterize objects. All information relating to the objects will be encapsulated in separate classes and communication between objects will be achieved by calling member functions to manipulate the encapsulated data. This programming language is very modular in its programming which facilitates secondary development of it. The adaptation of the Hoek-Brown-PAC strain-softening model is mainly a modification of the existing constitutive code, which generates a dynamic link library (.dll) file of the custom constitutive model to be called before the initial in-situ stress step of FALC3D6.0 after a successful run. The development process consists mainly of the base class of the constitutive model, the definition of the corresponding membership functions, the registration of the model, the transfer of information between the constitutive model and FLAC3D during the loop, and the state degree indicator of the mesh. Newly created custom constitutive model projects contain two main file types: header file (.h) and source file (.cpp). The header file (.h) corresponds to the preprocessing block and contains the names of the classes and defined functions required in the present construction model as well as the names of the main parameters. The source file (.cpp) is the main file (the main execution step) that implements the target function of the program. The most important link between FLAC3D and the user-defined ontology in the source file (.cpp) is the member function of Run, which contains the update of the stress and strain tensor. When these functions are called, the stress component already contains the rotation correction term. The softening function is written by first specifying the elasticity instantiation involved in the embedding. Secondly, the new parameter GSI is added. Finally, the written function is embedded in the softening section of the Run function and run subsequently.

The flow of the program calculation mainly includes parameter initialization, solving for elastic strain and stress increments, yielding judgement, updating stress, strain and parameter values, etc. The specific flow chart can be presented in Fig. 3.

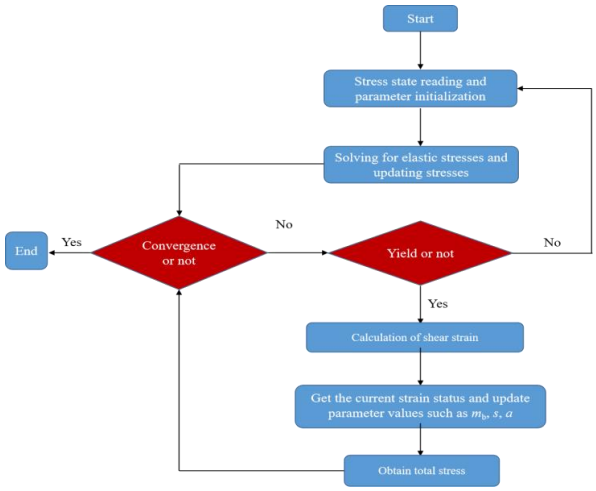

Fig. 3 Flow chart of the modified Hoek-Brown-PAC softening model calculation

Table 1 Values of η^* for different GSI and confining pressures

Confining pressure/MPa	GSI=60	GSI=50
3	0.00293822	0.004953184
6	0.004461406	0.009724744
9	0.006062466	0.015366104
Confining pressure/MPa	GSI=40	GSI=30
3	0.014891884	0.067734167
6	0.03600775	0.179538074
9	0.062322397	0.321639349

3.1 Realization of constitutive model

After compiling the cmodel custom constitutive model in VS2010, generated DLL file (cmodelhoekbrownpacd006_64. DLL) in the project folder corresponding to the "... \ VS2010 \ projects" path can be found. Subsequently, it is easy to copy the DLL file to the directory "... Itasca \ flac3d600 \ exe64 \ plugins \ cmodel".

The relevant statements used in the FLAC3D6.0 call include zone cmodel load ' cmodelHoekBrownPACd006_64.dll', model configure plugin and zone cmodel assign HoekBrownPAC. A commonly used numerical calculation model for tri-axial compression experiments is to be developed, as shown in Fig. 4. The model was built according to the standard specimen size (50 mm×100 mm) for the indoor tri-axial compression tests and the corresponding confining pressure is applied around the specimen. The top surface is velocity controlled. The loading speed is slowly raised from 0 to 1.0×10^{-5}m/s and held, with the bottom speed being 0 to achieve a fixed bottom. For better validation of the constitutive model, GSIs of 60, 50, 40 and 30 were selected, with confining pressures of 3 MPa, 6 MPa and 9 MPa respectively. For the value of η^*, the calculations in the previous sub-section can be shown in Table 1.

It is easy to see from Table 1 that η^* for GSI = 30 is much greater than the other values taken. Thus, the GSI is taken to be equal to 60 or 50 or 40. The GSI is equal to 30 when the confining pressure can be selected as a variable to achieve the verification of FLAC3D with the intended function by comparing the verification of the Hoek-Brown parameter with the function.

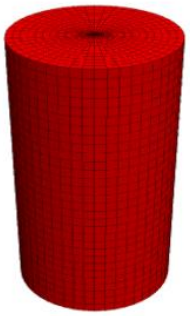

Fig.4 Specimen model

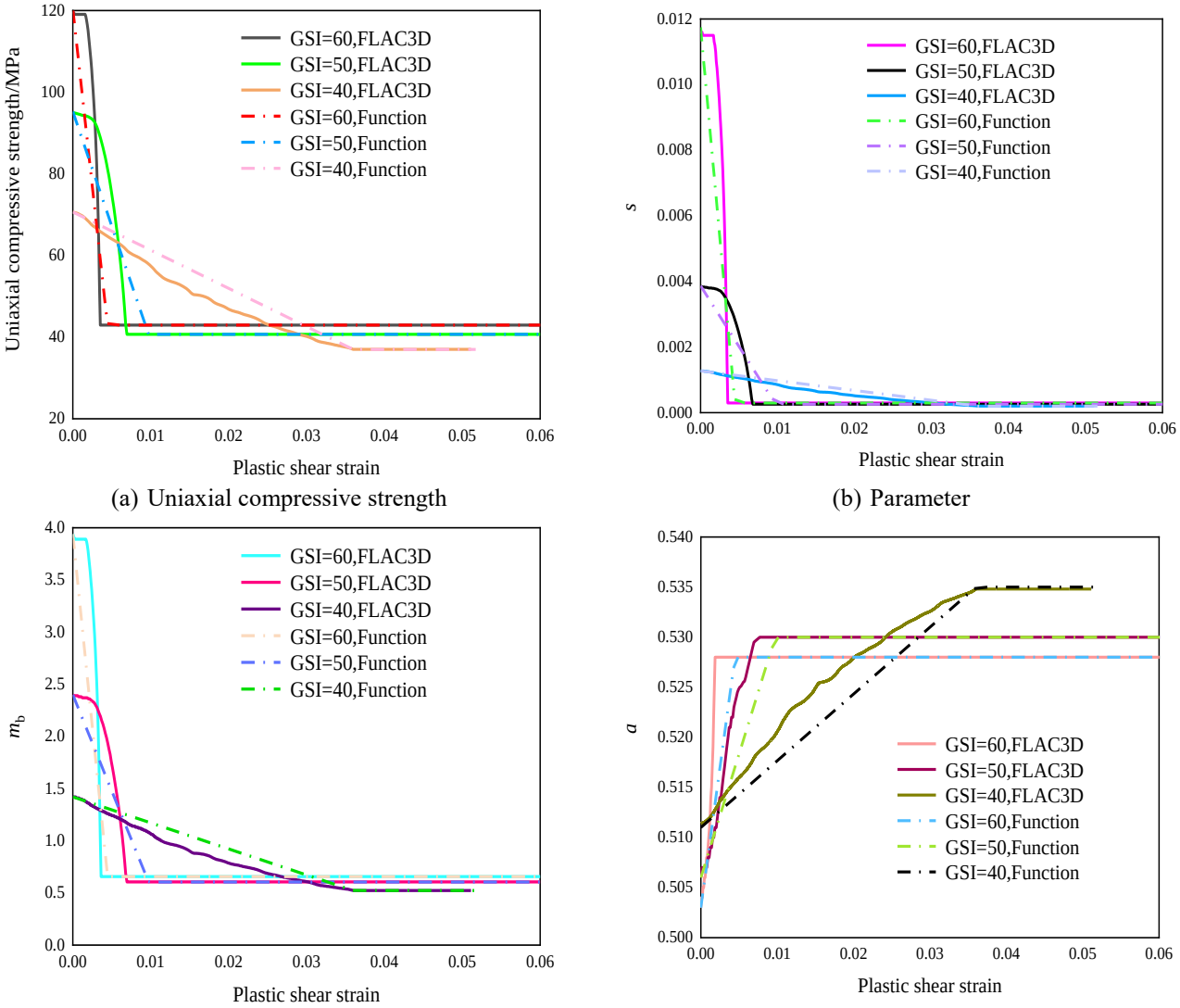

(a) Uniaxial compressive strength (b) Parameter

(c)m_b (d) Parameter *a*

Fig.5 Comparison between preset parameter functions and FLAC3D (confining pressure unchanged)

Fig. 5 presents the Hoek-Brown design functions for each parameter compared to the FLAC3D values for an confining pressure of 6 MPa. It is obvious to see that the values of the parameters in FLAC3D are consistent with the design values when it just enters the plastic and residual zones, with only some inconsistencies in the paths during the softening phase, which have little effect on the calculation results. Fig. 6 shows the effect of different confining pressures on the trend of each Hoek-Brown parameter at GSI = 30. Similar to Fig. 5, the design values for each parameter are relatively close to the FLAC3D values and the secondary development of the Hoek-Brown criterion can be considered to have achieved the design purpose.

Table 2 Links between RMR and GSI

Object	Documentary sources	The relationship between GSI and RMR
GSI,RMR	Hoek and Brown	GSI = RMR − 5
	Morales *et al.*	GSI = 4.714 + 0.687RMR
	Cosar	GSI = 0.42RMR + 23.07
	Osgoui and Ü nal	$GSI = 6e^{0.05RMR}$
	Hashemi *et al.*	GSI = 0.692RMR + 22.32
	Irvani *et al.*	GSI = 1.35RMR − 16.4
	Singh and Tamrakar	GSI = 0.73RMR − 4.38
	Ali *et al.*	GSI = 0.99RMR − 4.9
	Zhang *et al.*	GSI = 1.21RMR − 18.61
	Shahriar	GSI = 0.9143RMR+6.132

4. Verification of constitutive model

The best way to verify the feasibility of numerical simulation methods is to compare and analyze them with field measurements. The current Chinese code for the design of mountain tunnels starts with the classification of the surrounding rock in the path of excavation based on the [BQ] method in different geological conditions, followed by

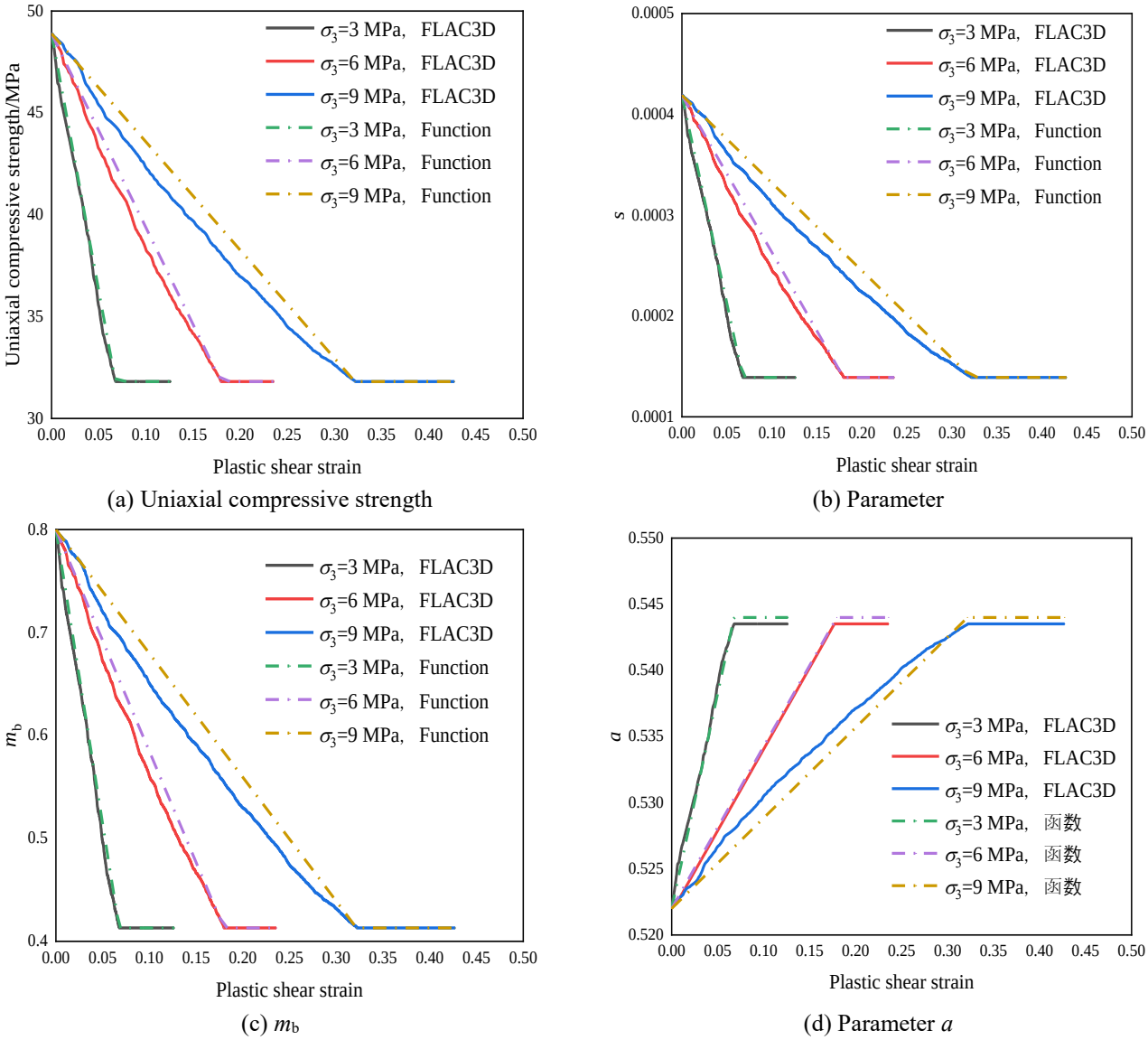

(a) Uniaxial compressive strength

(b) Parameter

(c) m_b

(d) Parameter *a*

Fig. 6 Comparison between preset parameter functions and FLAC3D (GSI unchanged)

Table 3 Recommended values for correction factors

Surrounding rock grade	I	II	III	IV	V
K1	0.1	0.15	0.3	0.55	0.7
K2	0.3	0.3	0.3	0.3	0.3
K3	0	0	0	0	0

Table 4 Correspondence table between GSI and BQ, [BQ]

Surrounding rock grade	I	II	III	IV	V
BQ or [BQ]	> 550	550-451	450-351	350-251	≤250
GSIBQ	≥72	71-55	54-39	38-23	≤22
GSI[BQ]	≥78	77-62	61-48	47-36	≤35

the determination of the excavation method and support parameters. If the secondary development results of the Hoek-Brown criterion described above are to be accurately put to the service of engineering practice, the stratigraphic parameters of the field must be accurately reflected in the numerical simulations. Thus, there is an urgent need to determine the equivalence of the GSI and [BQ] scores to ensure the accuracy of each parameter of the numerical simulation.

4.1 Equivalence method between GSI and [BQ]

There are few research results that reflect a direct link between GSI and [BQ] at this stage, which makes it impossible to obtain a direct equation for the relationship between GSI and [BQ]. Further research found that some of the results summarized the links between GSI and RMR, and BQ and RMR. Therefore, the relationship between GSI and [BQ] can be obtained by conversion using RMR as an intermediate transfer medium.

Table 5 Table of GSI values, rock properties corresponding to the surrounding rock grades

Surrounding rock grade	III	IV		V
[BQ]	450-351	350-251	251-168	≤167
GSI[BQ]	61-48	47-36	35-25	≤24
Rock property		Strain-Softening		Elastic-perfectly plastic

Table 6 Parameter table of the tunnel sections

Name	Parameter	Nianpan Tunnel	Dahongyan Tunnel
Tunnel	Span /m	11.88	12.48
	Height /m	9.57	9.83
	Initial in-situ stress /MPa	3.99	1.78
Shotcrete	Elastic modulus E_1 /GPa	25	
	Poisson's ratio	0.2	
	Thickness /m	0.1	0.22
Anchor	Elastic modulus E_b /GPa	206	
	Deformation modulus E_{st} /GPa		206
Steel arch	Cross-sectional area A_{set} /cm2	/	39.578
	Cross-sectional height h_{set} /mm		200
Secondary lining	Elastic modulus E_2 /GPa	30	
	Poisson's ratio	0.2	
	Thickness	0.35	0.45

Wu and Liu (2002) analyzed over 200 sets of base data in the field and found a good linear relationship between BQ values and RMR, with the relationship equation being

$$\mathrm{BQ} = 6.0943\mathrm{RMR} + 80.786 \tag{19}$$

In addition, the authors reviewed the foreign literature and summarized some of the equations for the relationship between RMR and GSI, as shown in Table 2. The GSI versus RMR fit curves obtained for RMRs of 10, 20, …, 100 are shown in Fig. 7.

From the fitted curve in Fig.7, the relationship between GSI and RMR can be expressed as

$$\mathrm{RMR} = 1.66\mathrm{GSI}^{\frac{1}{1.112}} \tag{20}$$

Substituting Eq. (20) into Eq. (19), the relationship between GSI and BQ can be obtained as

$$\mathrm{BQ} = 10.117\mathrm{GSI}^{\frac{1}{1.112}} + 80.786 \tag{21}$$

Regarding the correction coefficients K_1 for the influence of groundwater, K_2 for the influence of the production of the main structural surfaces and K_3 for the influence of the initial stress state, the engineering rock classification standard (2014) gives a range of values for different geological conditions. However, it is more difficult to determine the range of [BQ] for different surrounding rock conditions. Therefore, K_1 and K_2 will be taken as the average value. K_3 can be taken as 0 while there are fewer high in-situ stress environments in the tunnel monitoring section. The correction factors are then taken as shown in Table 3.

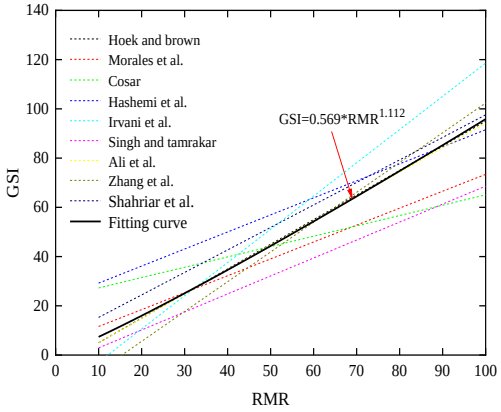

Fig. 7 Fitted curve between GSI and RMR

Substituting the range of [BQ] for different surrounding rock grades into Eq. (21) and referring to Table 3, the range of GSI under different surrounding rock grade tunnels can be obtained as shown in Table 4.

It shows that $\mathrm{GSI_{BQ}}$ and $\mathrm{GSI_{[BQ]}}$ are less than 22 and 36 respectively for rock classification as a Class V surrounding rock by comparing the scores of BQ and [BQ] converted to GSI. The GSI value of the general rock is 10 to 100, resulting in a low score for the BQ method of classifying soft and weak surrounding rocks, which is not conducive to designing for site construction. Thus, the [BQ] method is more rigorous than the BQ method of classification.

Table 7 Parameters' table of tunnel supports

Surrounding rock grade	Primary support				Secondary lining
	Bolt	Reinforcing Mesh	Shotcrete	Steel arch	
III	Diameter: Φ22 mm; Length:2.5 m; Inter-row spacing：120 cm×120 cm	Diameter: Φ8 mm; Interval: 25 cm×25 cm	Type: C25; Thickness: 10 cm	/	Type: C30; Thickness: 35 cm
V	Diameter: Φ22 mm; Length:3 m; Inter-row spacing: 120 cm×80 cm	Diameter: Φ8 mm; Interval:25 cm×25 cm	Type: C25; Thickness: 22 cm	Model: 18 cm-grille; Interval: 80 cm	Type: C30; Thickness: 45 cm

Table 8 Construction design parameters of the tunnels

Surrounding rock grade	Construction method	Distance of primary support (secondary lining) from excavation face/m	Cycle drilling /m
III	Full section method	6(90)	3.6
V	Three-step method	0(60)	3

Hoek and Brown (1997) found through extensive engineering practice that the post-peak mechanical behavior of a rock mass is related to the quality of the rock mass. The rock exhibits elastic-brittle damage when GSI > 75. When 25 < GSI < 75 and GSI < 25, the rock exhibits strain softening and elastic-perfectly plastic behavior after the peak, respectively. In view of the fact that the statistical monitoring sections are mainly distributed in the surrounding rock grades of Class III to Class V, corresponding to the GSI scores of 61 and below for the [BQ] method. Then the rock masses with higher surrounding rock grades mainly show strain softening and elastic-perfectly plastic behavior after the peak.

4.2 Relationships between GSI and Hoek Brown criterion parameters

In addition, the relationship between the GSI values and parameters m_b, s, α, σ_{ci} and E must be clarified. m_b,s and α are related to the GSI by Eqs. (2) and (3). Hoek and Diederichs (2006) proposed the relationship between σ_{ci} with GSI as follows.

$$\sigma_{ci} = \frac{0.5\exp(0.06\mathrm{GSI})}{0.0387 + 0.00474\exp(\mathrm{GSI}/18.9086)} \tag{22}$$

As for the elastic modulus E of rock, its deformation modulus E_m is generally measured, that is, the elastic modulus of rock and soil under unconfined conditions. Some scholars have obtained some results on the relationship between deformation modulus and GSI or RMR, as shown in Table 5. Zhou and Yang (2021) summarized many results and gave the following equation for fitting the elastic modulus E to the GSI.

$$E = 3.715\times10^{-4}\times\mathrm{GSI}^{2.72} \tag{23}$$

4.3 Validation of numerical simulations based on the secondary development of the Hoek-Brown criterion

Project sites are often dominated by Class III, IV and Vsurrounding rocks. The GSI corresponding to such surrounding rock classification can be listed in Table 5. The Nianpan Tunnel and Dahongyan Tunnel of Luanlu Highway Section-6 project were used as simulation objects. The Nianpan Tunnel and the Dahongyan Tunnel are dominated by Class III and V surrounding rocks respectively, which can represent strain-softening surrounding rock and elastic-perfectly plastic surrounding rock respectively.

The corresponding [BQ] values of Class III surrounding rock in the Nianpan Tunnel and Class V surrounding rock in the Dahongyan Tunnel are 351 and 128 respectively. According to Table 5, the corresponding GSIs are 48 and 17, respectively. The basic support parameters of the Nianpan Tunnel and the Dahongyan Tunnel are presented in Tables 6 and 7.

For the construction methods of the two tunnels, the full section and three-step methods are adopted for Class III and Class V surrounding rocks respectively. The heights of the upper, middle and lower sections of the three-step method are 2.45 m, 3 m and 4.38 m respectively, with the length of the upper step being 18 m and the length of the middle step being 27 m. The specific design parameters of tunnel constructions present as follows.

Due to the inconvenience of numerical modelling in FLAC3D 6.0 software, ABAQUS 6.14 finite element software was used to build the model for import and change the group name. A multi-centered circular tunnel is proposed, with a span of 12.48 m and a height of 9.83 m, based on the dimensions of a tunnel with a Class V surrounding rock. Half of the tunnel profile was taken for the modelling as it was considered that the gross tunnel profile is generally symmetrical along the center line. The model dimensions were set to 50 m×90 m×100 m with a number of units for 53021 due to boundary effects, and the resulting model is shown in Fig.8.

After the model was imported, the command flow of initial in-situ stress balance and construction steps was compiled with 'cmodelHoekBrownPACd006_64.dll'

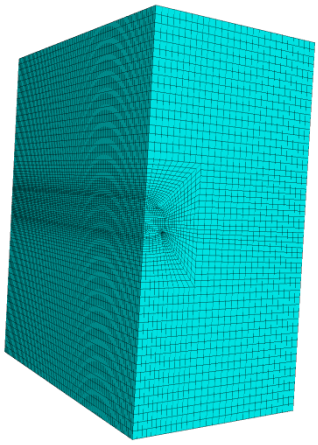

(a) Three-dimensional model

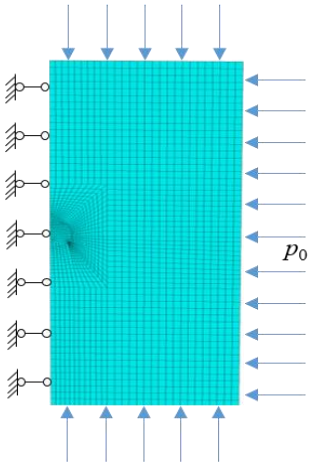

(b) Boundary conditions

Fig. 8 Schematic diagram of the calculation model

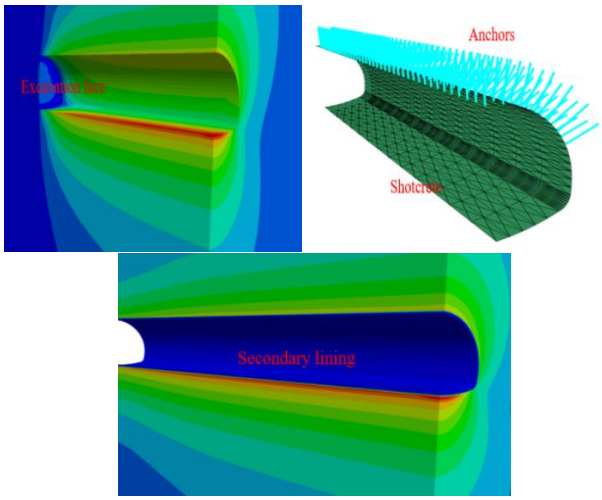

Fig. 9 Construction processes of Class III surrounding rock tunnel

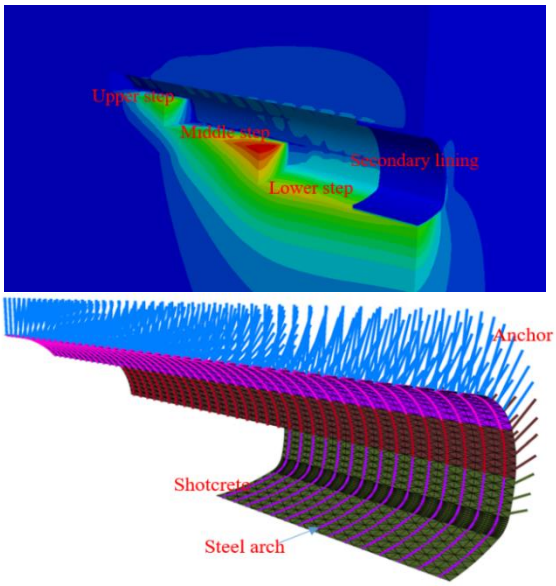

Fig. 10 Construction processes of Class V surrounding rock tunnel

imported at the time of initial in-situ stress balance. Initial in-situ stress balance included parameter input, output of historical data, boundary conditions, boundary displacement clearing and so on. The longitudinal middle section was taken as the monitoring section, and the vault and side wall of which were taken as the monitoring points. The left side, front side and back side of the model were constrained to their normal displacements, and the right side, bottom and top were applied with uniform loads, without considering the self-weight of the rock support structure. The construction steps included the initial in-situ stress balance, excavation of the rock mass and the application of supports, which were generally cyclic through the FISH language. For the simulation of the support structure, a Shell unit was created and assigned to the tunnel wall, which was shotcrete. If the anchor cannot resist the bending moment, Cable unit simulation was used. Beam units are isotropic, linear-elastic materials with no damage limits, and it can simulate steel arches. Moreover, the secondary lining generally used solid units, which were reflected in the modeling as secondary lining entities.

The main processes for the construction of Class III and V surrounding rocks can be presented in Figs. 9 and 10.

In addition, in order for the numerical simulation data to be as accurate as possible, it is necessary to consider the release of rock loads during the construction of the tunnels. Some scholars set artificial load release rates in their numerical simulations, which is obviously not rigorous. The released tunnel wall load is closely related to the primary support stiffness and the support time.The earlier the support or the greater the stiffness, the smaller the load release factor. Wang *et al*. (2019) used the volumetric loss control method to simulate stress release, reflecting the magnitude of stress release by the area of the surface settlement trough, which is applicable to shallow buried tunnels. Deep-buried tunnels generally reflect the depth of burial by applying a uniform load, which is essentially the same at the same boundary, and this method is not suitable for modelling deep-buried tunnels. Su *et al*. (2019) gave the section displacement release rate for different fenestration categories of tunnels at a distance of 0 from the excavation face, with a displacement release rate interval of 0.248 to 0.381, which is taken as 0.3 in this study. The displacement

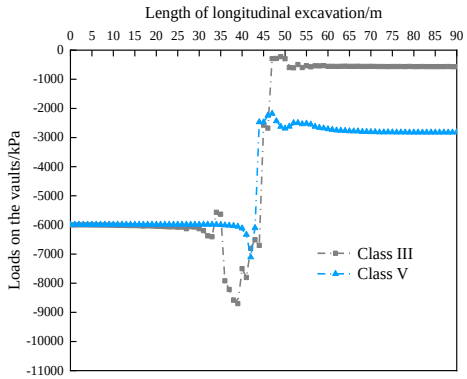

Fig. 11 Variation of load releases on the tunnel vaults

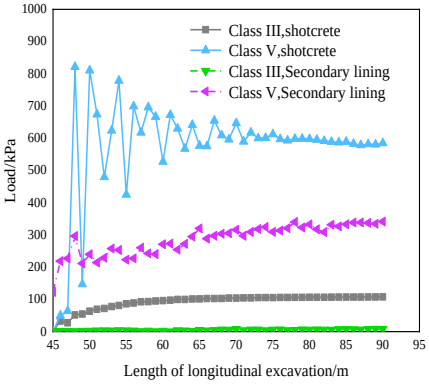

Fig. 12 Vertical loads of sprayed concrete

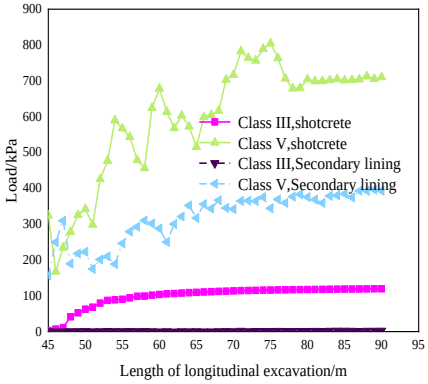

Fig. 13 Horizontal loads of sprayed concrete

release rate is taken as 0.65 for a Class III surrounding rock lag of 6 m.

Through continuous trial and error calculations, the corresponding cycles per cycle of rock excavation for Class III and V surrounding rocks are 110 and 25 respectively. Based on site experience, the slagging and de-risking time is approximately 6 hours. Likewise, the support time is approximately 1.2 times the excavation time with 132 and 30 cycles for Class III and V surrounding rocks respectively. The secondary lining is generally moulded once every two days, and the corresponding cycle is 880 and 200 for Class III and V surrounding rocks respectively.

The post-processing of the simulation resulted in the release of tunnel vault loads for different surrounding rock grades as shown in Fig. 11. The load on the vault at the monitoring point is essentially the same as the initial in-situ

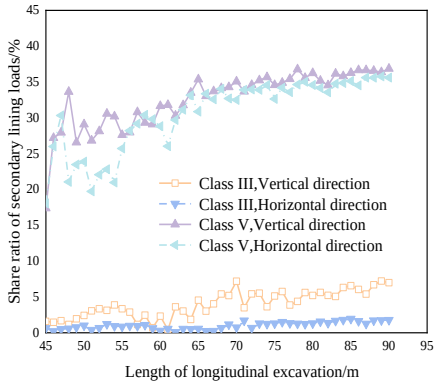

Fig. 14 Load sharing ratio of the secondary lining

stress when the excavation face has not yet advanced to the monitoring point. At a distance of 10 m from the monitoring point, the loads first increase and then drop significantly, which present a load release. After the excavation face passes the monitoring point, the load rises slightly and then stabilise. The worse the condition of the surrounding rock, the higher the vault load after stress relief. The surrounding loads for Class III and V surrounding rocks are 0.571 MPa and 2.814 MPa respectively, which shows that the support loads for Class V surrounding rock are higher.

Secondly, as the vault deformation in the field project is usually the deformation after the excavation of the monitoring section without the previous deformation, the direct comparison with the numerical simulation will be prone to deviation.Thus, the rationale for the secondary development of the Hoek-Brown criterion is illustrated by comparing the loads shared by the supports.

The loads shared between the shotcrete and the secondary lining are shown in Figs. 12 and 13. After the application of shotcrete or secondary lining, the contact load tends to increase, with fluctuations becoming more pronounced the higher the load. It is evident that the loads just after the installation of the secondary lining account for a larger proportion of the final load. The final loads on the vault and side walls of the Class III surround shotcrete are approximately 107.68 kPa and 119.47 kPa respectively. The final loads on the vault and side walls of the Class V surrounding rock shotcrete are approximately 585.03 kPa and 710.3 kPa respectively. The load sharing ratio of the secondary lining can be shown in Fig. 14. It can be seen that the load sharing ratio of the secondary lining on the vault of class III surrounding rock is greater than that of the side wall, reaching 7% while load sharing ratio at side wall of the Class V surrounding rock is greater than that of the vault, reaching 36.9%.

The field tests include the contact pressures between the surrounding rock and the primary support, and between the primary support and the secondary lining. The pressure boxes were placed at the side wall, arch waist and vault of the Nianpan Tunnel and the Dahongyan Tunnel. The monitoring instruments and the monitoring site are shown in Fig. 15.

The load sharing ratios for one section of each of the Dahongyan and Ninapan tunnels and the secondary lining are shown in Figs. 16 and 17 respectively. X is distance of

(a) Vibrating string type pressure box

(b) Frequency reader

(c) Between surrounding rock and primary support

(d) Between primary support and secondary lining

Fig. 15 Installation of the pressure boxes

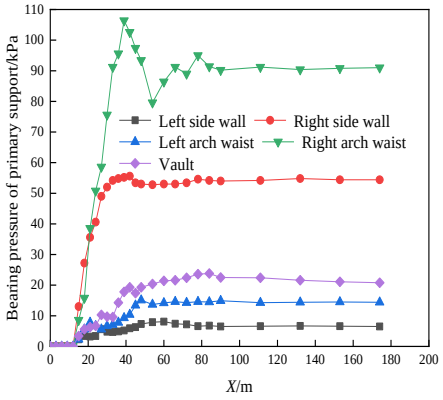

(a) Pressures on the primary support

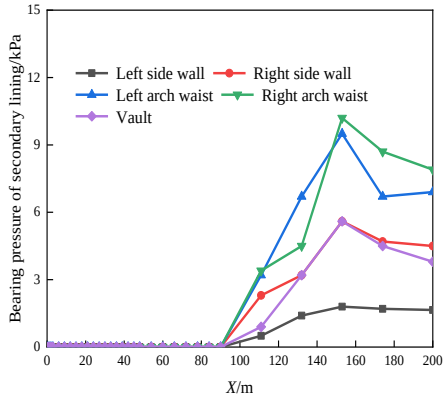

(b) Pressures on the secondary lining

Fig. 16 Pressure variation in the Nianpan Tunnel

the monitoring point from the excavation face. Fig. 16 shows the process that the pressure increases sharply-tends to be stable or even decreases slightly after the pressure box is installed. The maximum loads on the primary support and secondary lining appear at the right arch waist, and the loads are 91 kPa and 7.9 kPa respectively, which are within

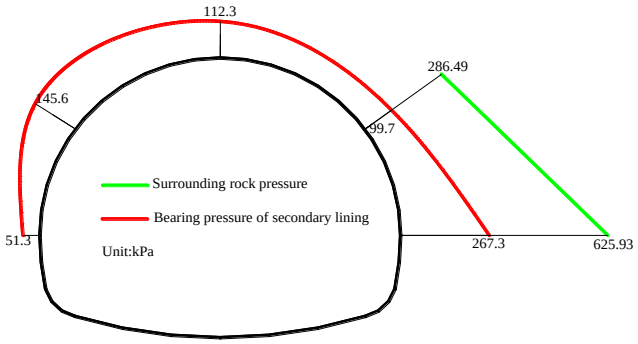

Fig. 17 Pressure values in the Dahongyan Tunnel

20% error compared to the numerical simulation results. For the load sharing ratio of the secondary lining, some monitoring points have a smaller load and a larger share of the secondary lining without reference. Since the location with large load is dangerous, the load sharing ratio of the secondary lining of the right arch waist is emphatically analyzed. The specific value of the secondary lining sharing ratio is 8.6%, which is close to the 7% of the numerical simulation with a small error. Fig. 17 shows the final loads on the primary support and the loads on the secondary lining at each monitoring point in a section of the Dahongyan Tunnel. The maximum loads on the primary support and secondary lining of the section were 625 kPa and 267.3 kPa respectively, and the error with the numerical simulation results was controlled to within 15%. The load sharing ratio at the maximum load is 29.9%, which is within 7% error compared to the numerical simulation results.

Numerical simulation and field monitoring belong to two research tunneling tools and the data often differ by a large margin, even by an order of magnitude. In summary, the numerical simulation load results from the secondary development of the Hoek-Brown criterion for this study were controlled to within 20% of the field monitoring error, verifying the feasibility of the secondary development.

In view of the above analysis, it was too slow to obtain the parameters for the rock experiments, which affected the project schedule. This study method enables rapid prediction of support loads in mountainous tunnels and is applicable to Class III surrounding rock conditions and worse. For hard rock conditions, numerical simulation prediction in this study is not necessary.

5. Analysis of factors influencing the support loads

The numerical simulations based on the secondary development of the Hoek-Brown criterion have been validated in the previous section, and it is also necessary to investigate the factors influencing the support loads, such as initial in-situ stress, support time, support stiffness, etc. This section plans to use Class III and V surrounding rocks as examples to analyse the influence of various factors on the support loads, which can be used to optimise the support design depending on the rock classification and geological conditions.

Table 9 support loads under different in-situ stress conditions

Surrounding rock grade	Initial in-situ stress /MPa	Monitoring point	Load sharing /kPa (The unit of anchor is kN)		
			Shotcrete	Secondary lining	Anchor
III	6	Vault	107.68	8.1	8.34
		Side wall	119.47	2.17	0
	9	Vault	122.3	14.3	10.76
		Side wall	128.8	3.25	4.55
	12	Vault	167.5	20.9	15.717
		Side wall	193.3	3.9	6.2
V	6	Vault	585.03	341.5	104.3
		Side wall	710.3	392.9	86.7
	9	Vault	712.4	524.3	123.7
		Side wall	824.7	684.7	88.6
	12	Vault	981.3	996.7	150.6
		Side wall	671.3	596.3	85.7

Table 10 Support load under different conditions of secondary lining construction time

Surrounding rock grade	Distance of the secondary lining lagging the excavation face /m	Monitoring point	Load sharing /kPa (The unit of anchor is kN)		
			Shotcrete	Secondary lining	Anchor
III	90	Vault	107.68	8.1	8.34
		Side wall	119.47	2.17	0
	80	Vault	109.23	8.21	8.24
		Side wall	108.47	2.17	0.2
	70	Vault	111.3	8.45	8.3
		Side wall	114.5	2.29	0.23
V	50	Vault	456.3	219.5	137.3
		Side wall	713.6	376.3	95.6
	40	Vault	585.03	341.5	104.3
		Side wall	710.3	392.9	86.7
	30	Vault	565.4	489.7	75.6
		Side wall	665.4	636.7	53.7

5.1 Initial in-situ stress

It is proposed to set the initial in-situ stress as a variable with 6 MPa, 9 MPa and 12 MPa for initial in-situ stress respectively. The load values shared by shotcrete, secondary lining and anchors for Class III and V surrounding rocks can be shown in Table 9. It is easy to see that as the initial in-situ stress increases, the load shared by the shotcrete and the secondary lining, the axial force of the anchor rod shows a tendency to increase, and the vault increases more than the side walls. The axial force of the sidewall anchors is close to zero in Class III surrounding rock, while the anchors in the vault of Class surrounding V rock are subject to greater axial forces, and the worse the rock conditions, the closer the axial force of the sidewall anchors is to the vault. The load sharing ratio of the secondary lining tends to increase, with the maximum load sharing ratios of 7.0% and 36.9% for Class III and Class V surrounding rocks respectively at a in-situ stress of 6 MPa. At a in-situ stress of 9 MPa, the maximum load sharing ratios are 10.5% and 45.4% for Class III and Class V surrounding rock secondary lining respectively. The maximum load sharing ratio of secondary lining of Class III and Class V surrounding rock is 11.1% and 50.4% respectively when the in-situ stress is 12 MPa.

5.2 Installation time

Since the shotcrete of Class IV and Class V surrounding rocks generally follows the tunnel face, priority should be given to setting the construction time of secondary lining as a variable. The distance between the secondary lining of Class III surrounding rock and the tunnel face is 90 m, 80 m and 70 m respectively. Correspondingly, the distance between the secondary lining of Class V surrounding rock and the tunnel face is 50 m, 40 m and 30 m respectively.

Then the loads shared by shotcrete, secondary lining and anchor of Class III and V surrounding rock are shown in

Table 11 Support loads for different time of primary support installation

Surrounding rock grade	Distance of the primary support lagging the excavation face /m /m	Monitoring point	Load sharing /kPa (The unit of anchor is kN)		
			Shotcrete	Secondary lining	Anchor
III	0	Vault	157.68	2.1	12.21
		Side wall	123.47	1.17	3.2
	6	Vault	107.68	8.1	8.34
		Side wall	119.47	2.17	0
	12	Vault	89.7	14.6	5.8
		Side wall	74.5	6.29	0

Table 12 Support loads for different secondary lining thickness conditions

Surrounding rock grade	Thickness of the secondary lining /m	Monitoring point	Load sharing /kPa (The unit of anchor is kN)		
			Shotcrete	Secondary lining	Anchor
III	0.4	Vault	107.68	8.1	8.34
		Side wall	119.47	2.17	0
	0.45	Vault	108.23	14.21	6.25
		Side wall	101.47	5.17	0.2
	0.5	Vault	101.3	23.45	4.16
		Side wall	98.5	8.29	0.23
V	0.5	Vault	585.03	341.5	117.4
		Side wall	727.9	306.7	76.7
	0.55	Vault	576.3	410.3	104.3
		Side wall	710.3	392.9	86.7
	0.6	Vault	516.3	513.4	96.7
		Side wall	712.4	601.3	85.6

Table 10. It is not difficult to see that the construction time of the secondary lining has little impact on the shotcrete load, but has a great impact on the secondary lining. The earlier the secondary lining is constructed, the greater the secondary lining load, the greater the secondary lining load sharing ratio, and the worse the surrounding rock conditions, the more obvious this trend is. The maximum interval of the load sharing ratio of the secondary lining of Class III surrounding rock is less than 10%, which indicates that the installation time of the secondary lining has little effect on the load sharing ratio of the Class III surrounding rock. The overall load sharing ratio on the secondary lining of the Class V surrounding rock is large, with the maximum second lining load sharing ratio ranging from 32.5% to 48.9%. Therefore, the installation time of the secondary lining has a significant impact on the soft rock, and the distance between the secondary lining and the tunnel face should be delayed if the primary support cannot encroach on the limit.

Since the shotcrete of Class IV and V surrounding rock generally follows the tunnel face, only the influence of construction time of Class III surrounding rock should be in consideration. The distance between the primary support of Class III surrounding rock and the tunnel face is 0 m, 6 m and 12 m respectively, so the loads shared by shotcrete, secondary lining and anchors of Class III surrounding rock is shown in Table 11 below. It is obvious to see that the construction time of primary support has a great impact on the load of shotcrete and little impact on the secondary lining. The earlier the primary support is constructed, the greater the load of shotcrete and the smaller the load sharing ratio of secondary lining. The maximum load sharing ratio range of secondary lining for Class III surrounding rock is less than 20%. The primary support can be appropriately delayed. It is recommended to apply the primary support once in two to three cycles to reduce the number of wet spraying and improve the construction efficiency.

5.3 Support stiffness

The requirements for shotcrete and secondary lining thickness vary for different rock grades of a tunnel when the thickness of the secondary lining and the thickness of the shotcrete as influencing variables were used. The thicknesses of the secondary lining are set at 0.4 m, 0.45 m and 0.5 m for Class III surrounding rock and 0.5 m, 0.55 m and 0.6 m for Class V surrounding rock at the same time.

The load values to be shared by shotcrete, secondary lining and anchors for Class III and V surrounding rocks can be shown in Table 12 below. It is easy to see from Table

Table 13 Support loads for different shotcrete thickness conditions

Surrounding rock grade	Thickness of the shotcrete /m	Monitoring point	Load sharing /kPa(The unit of anchor is kN)		
			Shotcrete	Secondary lining	Anchor
III	0.1	Vault	86.7	13.4	12.1
		Side wall	81.2	5.6	1.1
	0.15	Vault	107.68	8.1	8.34
		Side wall	119.47	2.17	0
	0.2	Vault	146.4	4.3	5.4
		Side wall	135.6	1.2	0
V	0.2	Vault	487.8	487.4	145.6
		Side wall	584.5	636.7	103.4
	0.25	Vault	585.03	341.5	104.3
		Side wall	710.3	592.9	86.7
	0.3	Vault	728.6	298.2	75.4
		Side wall	853.4	689.3	34.5

12 that the thickness of the secondary lining also has a small effect on the shotcrete load and the axial force of the anchors, while the load effect on the secondary lining is larger. The thicker the secondary lining, the greater the load on the secondary lining and the greater the load sharing ratio of the secondary lining, and the worse the surrounding rock conditions, the more obvious this trend becomes. The maximum interval of the secondary lining load sharing ratio is greater than 20% when the thickness of the secondary lining is 0.5 m, which indicates that the thickness of the secondary lining has an increasing effect on the secondary lining load of the Class III surrounding rock. However, Class III surrounding rock destabilization is rare and there is generally no increase in the thickness of the secondary lining. The secondary lining load sharing ratio of the Class V surrounding rock is generally large, with a maximum secondary lining load sharing ratio range of 32.8% to 45.8%. As a result, the thickness of the secondary lining has a greater impact on the soft surrounding rock, with a slightly smaller effect than the installation time of the secondary lining.

The proposed shotcrete thicknesses are 0.1 m, 0.15 m and 0.2 m for Class III surrounding rock and 0.2 m, 0.25 m and 0.3 m for Class V surrounding rock. The load values to be shared by shotcrete, secondary lining and anchors for Class III and V surrounding rocks are shown in Table 13 below. The thickness of the shotcrete has a greater effect on its load and the axial force of the anchors with less the effect on the load of the secondary lining. The thicker the shotcrete, the greater its load and the smaller the load sharing ratio of the secondary lining, and the worse the surrounding rock conditions, the more pronounced this trend becomes. The minimum load sharing ratio of the surrounding rock is less than 1% when the thickness of the Class III surrounding rock is 0.2 m which indicates that the effect of increasing the shotcrete thickness of the Class III surrounding rock is not obvious. It cannot affect the primary support as the main load-bearing structure which will increase costs and should be avoided. The overall load sharing ratio of the secondary lining is larger for Class V surrounding rock, and the maximum secondary lining load sharing ratio is reduced by 18.1% when the shotcrete thickness is increased by 0.1 m. The effect is further improved. In summary, the thickness of the shotcrete has a significant effect on the secondary lining load of the soft surrounding rock.

Based on this, it is probable that the thicker and earlier the secondary lining is applied, the more likely it is that the secondary lining will become the main load-bearing structure for the Class V surrounding rock. The reduced stiffness of the primary support will make the secondary lining more visible as a primary load bearing structure. Therefore, the primary support stiffness must be ensured as far as cost allows, while the primary support stiffness of Class III surrounding rock can be designed according to the specifications.

6. Conclusions

In this study, the load pattern of the surrounding rock is analyzed by modifying the self-strain softening constitutive model based on the Hoek-Brown criterion for deep-buried tunnels, which embedded segmental equations containing the variation of each parameter with the softening factor and conclusions are as follows.

(1) The smaller the GSI or the greater the confining pressure, the greater the change η^* value. When GSI > 45, the effect of the confining pressure on η* is small and it is recommended that the effect of the confining pressure on η^* can be ignored when the confining pressure is less than 10 MPa. However, we should pay attention to the parameter of confining pressure when GSI < 45. The relationship between η* and GSI is given by curve fitting of the form $\eta^*=z_1\times(\sigma_3)^{z_2}$. Equations are given for the main parameters of the Hoek-Brown criterion σ_{ci}, m_b, s and a in relation to the plastic strain η, the surrounding pressure and

the GSI, which is embedded in the Hoek-Brown-PAC constitutive model.

(2) A comparison of the paths in the main parameters σ_{ci}, m_b, s and a of the Hoek-Brown criterion with the plastic strain in FLAC3D shows that the values of the parameters are consistent with the design values just after entering the plastic and residual zones, with only some inconsistencies in the paths during the softening phase, which have little effect on the calculation results. The design values for each parameter are closer to the FLAC3D simulation results and the secondary development of the Hoek-Brown criterion meets the design objectives.

(3) The anchor axial forces in the vault, arch waist and side wall of the Class V surrounding rock are high and the anchor support is significant. The anchor shaft force is greatest in the vault of Class III surrounding rock, while the side wall is the smallest, close to 0. The role of the anchor in the side wall is not obvious and the anchor may not be installed to reduce the cost.

(4) For Class V surrounding rock, the thicker and earlier the secondary lining is applied, the more likely it is that the secondary lining will become the main load-bearing structure. The reduced stiffness of the primary support will make the secondary lining more visible as a primary load bearing structure. Thus, the primary support stiffness must be ensured as far as cost allows, while the primary support stiffness of Class III surrounding rocks can be designed according to the specifications.

Acknowledgments

The authors acknowledge the Scientific Research Project of Zhejiang Provincial Transportation Department (2021050) for the preparation of this manuscript. This financial support is greatly appreciated.

References

Alejano, L.R., Alonso, E., Rodriguez-Dono, A. and Fernandez-Manin, G. (2010), "Application of the convergence-confinement method to tunnels in rock masses exhibiting Hoek-Brown strain-softening behavior", *Int. J. Rock. Mech. Min. Sci.*, **47**(1), 150-160. https://doi.org/10.1016/j.ijrmms.2009.07.008.

Arzua, J. and Alejano, L.R. (2013), "Dilation in granite during servo-controlled triaxial strength tests", *Int. J. Rock. Mech. Min. Sci*., **61**, 43-56. https://doi.org/10.1016/j.ijrmms.2013.02.007.

Ali, W., Mohammad, N. and Tahir, M. (2014), "Rock mass characterization for diversion tunnels at diamer Basha Dam, Pakistan-a design perspective", *Int. J. Sci. Eng. Technol*., **3**(10), 1292-1296.

Arzua, J., Alejano, L.R. and Walton, G. (2014), "Strength and dilation of jointed granite specimens in servo-controlled triaxial tests", *Int. J. Rock. Mech. Min. Sci.*, **69**, 93-104. https://doi.org/10.1016/j.ijrmms.2014.04.001.

Bagheripour, M.H., Rahgozar, R., Pashnesaz, H. and Malekinejad, M. (2011), "A complement to Hoek-Brown failure criterion for strength prediction in anisotropic rock", *Geomech. Eng.*, **3**(1), 61-81. https://doi.org/10.12989/gae.2011.3.1.061.

Bertuzzi, R., Douglas, K. and Mostyn, G. (2016), "Comparison of quantified and chart GSI for four rock masses", *Eng. Geol.*, **202**, 24-35. https://doi.org/10.1016/j.enggeo.2016.01.002.

Cai, M. (2010), "Practical estimates of tensile strength and Hoek-Brown Strength Parameter m(i) of Brittle Rocks", *Rock. Mech. Rock. Eng.*, **43**(2), 167-184. https://doi.org/10.1007/s00603-009-0053-1.

Cai, M., Kaiser, P.K., Tasaka, Y. and Minami, M. (2007), "Determination of residual strength parameters of jointed rock mass using the GSI system", *Int. J. Rock. Mech. Min. Sci.*, **44**, 247-265. https://doi.org/10.1016/j.ijrmms.2006.07.005.

Cai, W.Q., Zhu, H.H., Liang, W.H. (2022), "Three-dimensional tunnel face extrusion and reinforcement effects of underground excavations in deep rock masses", *Int. J. Rock. Mech. Min. Sci.* **150**, 104999. https://doi.org/10.1016/j.ijrmms.2021.104999.

Campos, L.A., Ferreira, F.A., Costa, T.A.V. and Marques, E.A.G. (2020), "New GSI correlations with different RMR adjustments for an eastern mine of the Quadrilatero Ferrifero", *J. S. Am. Earth. Sci.*, **102**, 102647. https://doi.org/10.1016/j.jsames.2020.102647.

Cosar, S. (2004), "Application of rock mass classification systems for future support design of the dim tunnel near Alanya", Master of Science thesis in mining engineering, Middle East Technical University, Ankara Turkey.

Chinaei, F., Ahangari, K. and Shirinabadi, R. (2021), "Hoek-Brown failure criterion for damage analysis of tunnels subjected to blast load", *Geomech. Eng.*, **26**(1), 41-47. https://doi.org/10.12989/gae.2021.26.1.041.

Cui, L., Sheng, Q., Zheng, J.J., Cui, Z. and Shen, Q. (2019), "Regression model for predicting tunnel strain in strain-softening rock mass for underground openings", *Int. J. Rock. Mech. Min. Sci.*, **119**, 81-97. https://doi.org/10.1016/j.ijrmms.2019.04.014.

Gomes, G.J.C., Forero, J.H., Vargas, E.A. and Vrugt, J.A. (2021), "Bayesian inference of rock strength anisotropy: Uncertainty analysis of the Hoek-Brown failure criterion", *Int. J. Rock. Mech. Min. Sci.*, **148**, 104952. https://doi.org/10.1016/j.ijrmms.2021.104952.

Gu, X., Chen, F.Y., Zhang, W.A., Wang, Q. and Liu, H.L. (2022), "Numerical investigation of pile responses induced by adjacent tunnel excavation in spatially variable clays", *Undergr. Space*, **7**(5), 911-927. https://doi.org/10.1016/j.undsp.2021.09.003.

Gu, X., Ou Q., Zhang W.G., Fu, J. and Hao, S.L. (2023), "A novel subroutine for estimating unsaturated slope stability considering reservoir water fluctuation in spatially variable soils", *B. Eng. Geol. Environ.*, **82**(6). https://doi.org/10.1007/s10064-022-03025-y.

Han, L., Liu, H.L., Zhang, W.A., Ding, X.M., Chen, Z.X., Feng, L. and Wang, Z, Y. (2022), "Seismic behaviors of utility tunnel-soil system: with and without joint connections", *Undergr. Space*, **7**(5), 798-811. https://doi.org/10.1016/j.undsp.2021.08.001.

Hashemi, M., Moghaddas, S. and Ajalloeian, R. (2010), "Application of rock mass characterization for determining the mechanical properties of rock mass: A comparative study", *Rock. Mech. Rock. Eng.*, **43**(3), 305-320. https://doi.org/10.1007/s00603-009-0048-y.

Hoek, E., Carranza-Torres, C. and Corkum, B. (2002), "Hoek-Brown failure criterion——2002 edition", *Proceedings of the 5th North American Rock Mechanics Symposium and 17th Tunneling Association of Canada Conference*, Toronto.

Hoek, E. and Brown, E.T. (1997), "Practical estimates of rock mass strength", *Int. J. Rock. Mech. Min. Sci.*, **34**, 1165-1186. https://doi.org/10.1016/S0148-9062(97)00305-7.

Hoek, E. and Diederichs, M.S. (2006), "Empirical estimation of

rock mass modulus", *Int. J. Rock. Mech. Min. Sci.*, **43**, 203-215. https://doi.org/10.1016/j.ijrmms.2005.06.005.

Huang, S., Hu, S.H., Zhao, L.H. and Zeng, Z.L. (2021), "Stability analysis of deep rectangular tunnels using adaptive finite element limit analysis with Hoek–Brown failure criterion", *Aba. J. Sci. Eng.*, **46**(11), 10931-10941. https://doi.org/10.1007/s13369-021-05632-5.

Industry standard compilation group of the people's Republic of China. (2015), "GB/T 50218–2014 Standard for engineering classification of rock mass", Beijing, China Planning Press.

Ismael, M. and Konietzky, H. (2019), "Constitutive model for inherent anisotropic rocks: Ubiquitous joint model based on the Hoek-Brown failure criterion", *Comput. Geotech.*, **105**, 99-109. https://doi.org/10.1016/j.compgeo.2018.09.016.

Irvani, I., Wilopo, W. and Karnawati, D. (2013), "Determination of nuclear power plant site in West Bangka based on rock mass rating and geological strength index", *J. South. Asian. Appl. Geol.*, **5**(2), 78-86.

Jin, J.C. (2020), "A finite element implementation of the strain-softening model based on the Hoek-Brown Criterion", *Eng. Mech*., **37**(1), 43-52. https://doi.org/1000-4750(2020)37:1<43:JYHBZZ>2.0.TX;2-D.

Kabwe, E., Karakus, M., Chanda, E.K. (2019), "Proposed solution for the ground reaction of non-circular tunnels in an elastic-perfectly plastic rock mass", *Comput. Geotech*., **119**, 103354. https://doi.org/10.1016/j.compgeo.2019.103354.

Laderian, A. and Abaspoor, M.A. (2012), "The correlation between RMR and Q systems in parts of Iran", *Tunn. Undergr. Sp. Tech.*, **27**(1), 149–158. https://doi.org/10.1016/j.tust.2011.06.001.

Li, W.T. (2012), The post-peak strain softening constitutive it equation and numerical simulation of rock, Shandong University, Jinan.

Merifield, R.S., Lyamin, A.V. and Sloan, S.W. (2006), "Limit analysis solutions for the bearing capacity of rock masses using the generalised Hoek-Brown criterion", *Int. J. Rock. Mech. Min. Sci.*, **43**(6), 920–937. https://doi.org/0.1016/j.ijrmms.2006.02.001.

Li, T.Z. and Yang, X.L. (2019), "Face stability analysis of rock tunnels under water table using Hoek-Brown failure criterion", *Geomech. Eng*., **18**(3), 235-245. https://doi.org/10.12989/gae.2019.18.3.235.

Morales, T., Uribe-Etxebarria, G., Uriarte, J.A. and de Valderrama, I.F. (2004), "Geomechanical characterisation of rock masses in alpine regions: the Basque arc (Basque-Cantabrian basin, northern Spain)", *Eng. Geol*., **71**(3-4), 343-362. https://doi.org/10.1016/S0013-7952(03)00160-1.

Osgoui, R. and Ünal, E. (2005), "Rock reinforcement design for unstable tunnels originally excavated in very poor rock mass", *Proceedings of the 31st ITAAITES World Tunnel Congress*, Istanbul, Turkey.

Qin, S., Shao, Z.S., Yuan, B., Zheng, X.M., Zhao, N.N. and Wu, K. (2023), "A simple prediction model for mechanical response of lined tunnels incorporating yielding elements", *Int. J. Appl. Mech*., **15**(5), 2350031. https://doi.org/10.1142/S175882512350031X.

Ranjbarnia, M., Rahimpour, N. and Oreste, P. (2020), "A new analytical-numerical solution to analyze a circular tunnel using 3D Hoek-Brown failure criterion", *Geomech. Eng.*, **22**(1), 11-23. https://doi.org/ 10.12989/gae.2020.22.1.011.

Sadeghi, S., Teshnizi, E.S. and Ghoreishi, B. (2020), "Correlations between various rock mass classification/ characterization systems for the Zagros tunnel-W Iran", *J. Mount. Sci.*, **17**(7), 1790-1806. https://doi.org/10.1007/s11629-019-5665-7.

Singh, J.L. and Tamrakar, N.K. (2013), "Rock mass rating and geological strength index of rock masses of Thopal-Malekhu River areas, central Nepal lesser Himalaya", *Bull. Depart. Geol.*, **16**, 29-42.

Somodi, G., Bar, N., Kovacs, L., Arrieta, M., Torok, A. and Vasarhelyi, B. (2021), "Study of rock mass rating (RMR) and geological strength index (GSI) correlations in granite, siltstone, sandstone and quartzite rock masses", *Appl. Sci.*, **11**(8), 3351. https://doi.org/10.3390/app11083351.

Su, K., Zhang, Y.J., Wu, H.T. and Zhou, L. (2019), "Evolution of surrounding rock safety factor and support installation time during tunnel excavation", *Chi. J. Rock. Mech. Eng.*, **38**(1), 2964-2975.

Ukritchon, B. and Keawsawasvong, S. (2019), "Stability of unlined square tunnels in Hoek-Brown rock masses based on lower bound analysis", *Comput. Geotech.*, **105**, 249-264. https://doi.org/10.1016/j.compgeo.2018.10.006.

Wang, S.L., Yin, X.T., Tang, H. and Ge, X.R. (2010), "A new approach for analyzing circular tunnel in strain-softening rock masses", *Int. J. Rock. Mech. Min. Sci*., **47**(1), 170-178. https://doi.org/10.1016/j.ijrmms.2009.02.011.

Wan, T., Han, X., Su, K. and Zhu, Y.S. (2019), "Numerical simulation methods and engineering applications of FLAC3D - An in-depth analysis of FLAC3D 5.0", Beijing, China Architecture & Building Press.

Wang, Y.N. (2018), "Study on strain softening mechanism and stability control of deep roadway surrounding rock", China University of Mining and Technology, Xuzhou.

Wu, A.Q. and Liu, F.Z. (2012), "Advancement and application of the standard of engineering classification of rock masses", *Chi. J. Rock. Mech. Eng.* **31**(8), 1513-1523.

Wu, K. and Shao, Z.S. (2019), "Study on the effect of flexible layer on support structures of tunnel excavated in viscoelastic rocks", *J. Eng. Mech.*, **145**(10), 04019077. https://doi.org/10.1061/(ASCE)EM.1943-7889.0001657.

Wu, K., Shao, Z.S. and Qin, S. (2020), "An analytical design method for ductile support structures in squeezing tunnels", *Arch. Civ. Mech. Eng.*, **20**(3), 91. https://doi.org/10.1007/s43452-020-00096-0.

Wu, K., Shao, Z.S., Jiang, Y.L., Zhao, N.N., Qin, S. and Chu, Z.F. (2023a), "Determination of stiffness of circumferential yielding lining considering the shotcrete hardening property", *Rock Mech. Rock Eng.*, **56**(4), 3023-3036. https://doi.org/10.1007/s00603-022-03122-0.

Wu, K., Sharifzadeh, M., Shao, Z.S., Zhao, N.N. and Yang, Y.Z. (2023b), "Analytical model for soft rock tunnel with large deformation using rigid and yielding lining solutions", *Int. J. Geomech.*, **23**(9). https://doi.org/10.1061/IJGNAI.GMENG-8483.

Wu, K., Shao, Z.S., Sharifzadeh, M., Hong, S.Y. and Qin, S. (2022a), "Analytical computation of support characteristic curve for circumferential yielding lining in tunnel design", *J. Rock Mech. Geotech. Eng.*, **14**(1), 144-152. https://doi.org/10.1016/j.jrmge.2021.06.016.

Wu, K., Shao, Z.S., Sharifzadeh, M., Chu, Z.F. and Qin, S. (2022b), "Analytical approach to estimating the influence of shotcrete hardening property on tunnel response", *J. Eng. Mech.*, **148**(1), 04021127. https://doi.org/10.1061/(ASCE)EM.1943-7889.0002052.

Wu, K., Shao, Z.S., Qin, S., Zhao, N.N. and Chu, Z.F. (2021a), "An improved non-linear creep model for rock applied to tunnel displacement prediction", *Int. J. Appl. Mech.,* **13**(8), 2150094. https://doi.org/10.1142/S1758825121500940.

Wu, K., Shao, Z.S., Qin, S., Wei, W. and Chu, Z.F. (2021b), "A critical review on the performance of yielding supports in squeezing tunnels", *Tunn. Undergr. Sp. Tech*., **115**, 103815. https://doi.org/10.1016/j.tust.2021.103815.

Xu, G.W., Gutierrez, M., Arora, K. and Wang, X. (2022), "Visco-

plastic response of deep tunnels based on a fractional damage creep constitutive model", *Acta. Geotech.*, **17**(2), 613-633. https://doi.org/10.1007/s11440-021-01226-5.

Yang, X.L., Zhou, T. and Li, W.T. (2018), "Reliability analysis of tunnel roof in layered Hoek-Brown rock masses", *Comput. Geotech.*, **104**, 302-309. https://doi.org/10.1016/j.compgeo.2017.12.007.

Zareifard, M.R. (2020), "A new semi-numerical method for elastoplastic analysis of a circular tunnel excavated in a Hoek-Brown strain-softening rock mass considering the blast-induced damaged zone", *Comput. Geotech*., **122**, 103476. https://doi.org/10.1016/j.compgeo.2020.103476.

Zhang, Q., Huang, X., Zhu, H. and Li, J.C. (2019), "Quantitative assessments of the correlations between rock mass rating (RMR) and geological strength index (GSI)", *Tunn. Undergr. Sp. Tech.*, **83**, 73-81. https://doi.org/10.1016/j.tust.2018.09.015.

Zhao, N.N., Shao, Z.S., Chen, X.Y., Yuan, B. and Wu, K. (2022a), "Prediction of mechanical response of a flexible support system supported tunnel in viscoelastic geomaterials", *Arch. Civ. Mech. Eng.*, **22**(4), 160. https://doi.org/10.1007/s43452-022-00485-7.

Zhao, N.N., Shao, Z.S., Yuan, B., Chen, X.Y. and Wu, K. (2022b), "Analytical approach to the coupled effects of slope angle and seepage on shallow lined tunnel response", *Int. J. Appl. Mech.*, **14**(2), 2250003. https://doi.org/10.1142/S175882512250003X.

Zhao, N.N., Shao, Z.S., Chen, X.Y., Yuan, B. and Wu, K. (2023a), "Analytical approach to estimating the influence of friction slip contact between surrounding rock and concrete lining on mechanical response of deep rheological soft rock tunnels", *Appl. Math. Model.*, **113**, 287-308. https://doi.org/10.1016/j.apm.2022.09.012.

Zhao, N.N., Shao, Z.S. and Wu, K. (2023b), "Analytical approach to predicting the time-dependent response of deep soft rock tunnels considering the compressible layer and stress path effects", *Int. J. Geomech.*, **23**(6), 04023070. https://doi.org/10.1061/IJGNAI.GMENG-8099.

Zhou, J. and Yang X.A. (2021), "Deformation behavior analysis of tunnels opened in various rock mass grades conditions in China", *Geomech. Eng.*, **26**(2), 191-204. https://doi.org/10.12989/gae.2021.26.2.191.

Zhu, X.P. (2015), "The Secondary development of FLAC3D based on jointed rock mass damage model and its application", China University of Geosciences, Beijing.

Zou, J.F., Zuo, S.Q. and Xu, Y. (2016), "Solution of strain-softening surrounding rock in deep tunnel incorporating 3D Hoek-Brown failure criterion and flow rule", *Math. Probl. Eng.*, 7947036. https://doi.org/10.1155/2016/7947036.